the folded Yukawa potential have been published e.g. by Möller and Nix (1981).

In the modified oscillator potential there are basically three parameters, $\omega_0$, $\kappa$ and $\mu$ for each kind of nucleon. If we for the moment neglect the neutron–proton differences of the three parameters, $\omega_0$ is used to determine the radius of the resulting matter distribution (from the wave functions of the occupied orbitals), $\mu$ or rather $\mu' = \kappa\mu$ can be viewed as simulating the surface diffuseness depth, and $\kappa$ is the spin–orbit coupling strength.

To illustrate further the effect of the $\boldsymbol{\ell} \cdot \mathbf{s}$- and $\boldsymbol{\ell}^2$-terms, we show on the left in fig. 6.3 the pure harmonic oscillator levels. Next is shown how the term $-\mu'\hbar\omega_0[\boldsymbol{\ell}^2 - N(N+3)/2]$ energetically favours high-$\ell$ subshells. Finally, in the third column of levels a spin–orbit term $-2\kappa\hbar\omega_0\boldsymbol{\ell} \cdot \mathbf{s}$ has been added. The values of $\kappa$ and $\mu'$ are roughly those that fit the neutrons in the ${}^{208}_{82}\mathrm{Pb}_{126}$ region of nuclei as to level order etc. To make the same diagram applicable with somewhat improved accuracy in the lighter-element region, smaller $\mu'$-values and somewhat larger $\kappa$-values have been used in the plot for the lower shells, as indicated in the figure. (This is roughly the same fit as made by Nilsson (1955).)

In the applications of the following chapters, we will mainly concentrate on the modified oscillator (MO) potential. This is so because the physical effects we want to illustrate come out in a similar way in all reasonable potentials (or Hartree–Fock calculations) and then we want to add as few calculational difficulties as possible. To conclude this chapter, we will discuss the parameters of the MO potential and the experimental information used for their determination in some detail.

## 6.3 The nuclear volume parameter

Let us first consider the parameter $\omega_0$ of the MO (modified oscillator) potential. The radial coordinate of the nuclear wave function is $(M\omega_0/\hbar)^{1/2} \cdot r$. The characteristic length is thus $(\hbar/M\omega_0)^{1/2}$. From the wave functions we may calculate a total nuclear density as a sum of all the single-particle densities from which the average radius could be further studied and compared with experiments. A simply accessible quantity for oscillator wave functions (or for any wave function that is given in an oscillator basis) is, however

$$\left\langle r_i^2 \right\rangle = \left(N_i + \frac{3}{2}\right) \frac{\hbar}{M\omega_0}$$

(see problem 6.8).

In terms of this we have already in preceding chapters defined an average

'root mean square radius' $R_{\text{rms}}$ as

$$R_{\text{rms}}^2 = \frac{5}{3}\langle r^2 \rangle = \frac{5}{3}\frac{1}{A}\sum_i \langle r_i^2 \rangle$$

We proceed to evaluate $\langle r \rangle^2$ for the case of filled oscillator shells. The degeneracy of an $N'$-shell is $(N'+1)(N'+2)$ (see problems), so for equal numbers of neutrons and protons, we have

$$A = 2\sum_{N'=0}^{N}(N'+1)(N'+2) \simeq 2\sum_{N'=0}^{N}(N'+3/2)^2$$
$$\simeq 2\int_{-1/2}^{N+1/2}(x+3/2)^2\,\mathrm{d}x \simeq \frac{2}{3}(N+2)^3$$

and

$$A\langle r^2 \rangle = 2\frac{\hbar}{M\omega_0}\sum_{N'=0}^{N}\left(N'+\frac{3}{2}\right)(N'+1)(N'+2) \simeq \frac{1}{2}\frac{\hbar}{M\omega_0}(N+2)^4$$

From these expressions we immediately obtain the relations

$$N+2 \simeq (3A/2)^{1/3}$$

and

$$R_{\text{rms}}^2 = \frac{5}{3}\frac{\hbar}{M\omega_0}\frac{1}{2}\left(\frac{3}{2}\right)^{4/3}\cdot A^{1/3}$$

Using the empirical value $R_{\text{rms}} = r_0 A^{1/3}$ with $r_0 = 1.2$ fm we obtain†

$$\hbar\omega_0 = \frac{\hbar^2}{Mr_0^2}\frac{5}{4}\left(\frac{3}{2}\right)^{1/3}\cdot A^{-1/3} \simeq 41\cdot A^{-1/3}\ \text{MeV}$$

The neutron and proton potentials are really different as shown in fig. 6.4. This is so although the neutron–neutron and proton–proton strong

† When calculating numerically the following expressions are useful

$$\frac{\hbar^2}{Mr_0^2} = 28.8\ \text{MeV}$$
$$r_0 = 1.2\ \text{fm}$$
$$m_e c^2 = 0.511\ \text{MeV}$$
$$M_p c^2 = 938.3\ \text{MeV}$$
$$M_n c^2 = 939.6\ \text{MeV}$$
$$\frac{e^2}{4\pi\varepsilon_0\hbar c} = \frac{1}{137}$$
$$\frac{e^2}{4\pi\varepsilon_0 r_0} = 1.2\ \text{MeV}$$

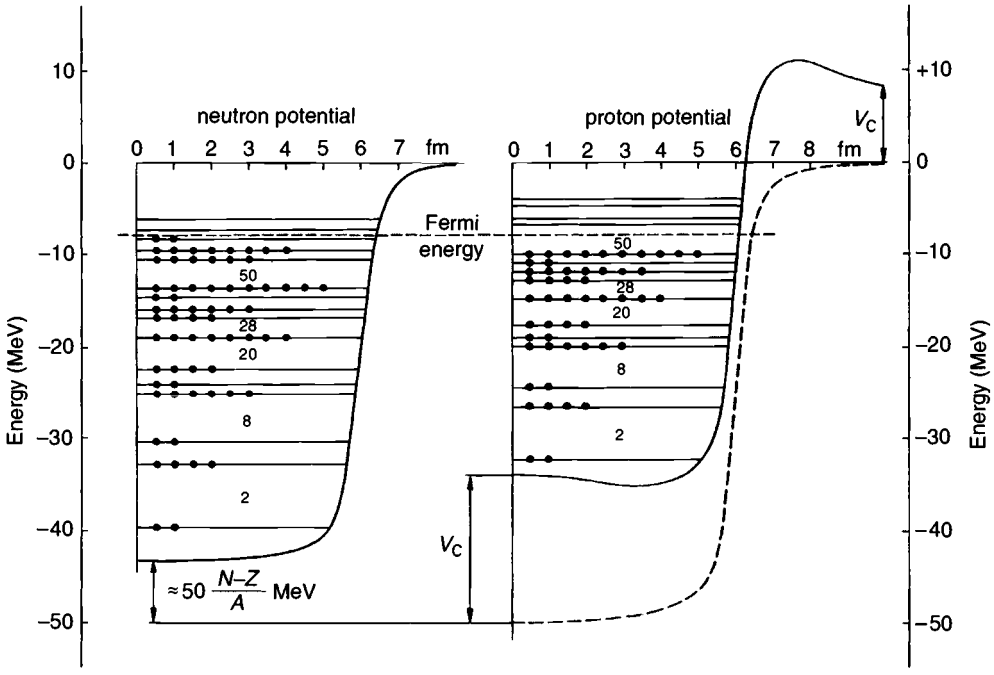


Fig. 6.4. The approximate neutron and proton potentials for $^{114}$Sn. As the 50 protons have more neighbours of the attractive opposite kind than the 64 neutrons have, the potential is deeper for the protons by $\simeq 50(N-Z)/A$ MeV. To this one has to add the Coulomb repulsive potential, which raises the total effective proton potential by nearly 20 MeV at the origin. The fact that the Fermi energy becomes the same for protons and neutrons leads to a neutron excess, which also comes out from the semi-empirical mass formula. The symmetry and Coulomb energies of this formula are directly related to the two differences between the proton and neutron potentials illustrated here.

two-body interactions are the same. The difference in the total one-body potential enters in two ways. First only the protons interact via the Coulomb force. In problem 6.11 we calculate the Coulomb potential inside and outside a homogeneous charge of radius $R = r_0 A^{1/3}$. The result is

$$V_C(r) = \begin{cases} \dfrac{Ze^2}{4\pi\varepsilon_0 R}\left(\dfrac{1}{2}\dfrac{r^2}{R^2} - \dfrac{3}{2}\right); & r < R \\ -\dfrac{Ze^2}{4\pi\varepsilon_0 r} \qquad\qquad ; & r > R \end{cases}$$

Inside $r = R$ the Coulomb potential is thus proportional to $r^2$, apart from a constant. It can thus very well be incorporated into the oscillator potential by a modification of $\omega_0$.

Actually, due to the repulsive Coulomb interaction, nuclei along the stability line have more neutrons than protons. It turns out that this has as a consequence that the protons move in a deeper nuclear potential than the neutrons (this is apart from the electromagnetic Coulomb repulsion). This is so because unlike particles bind each other better than like particles. Owing to the Pauli principle only half of the relative states accessible to unlike particles are also accessible to like particles. The protons furthermore have more unlike neighbours than the neutrons, and consequently a deeper potential results.

Both of these effects, the Coulomb and the Pauli principle effect, can be incorporated into the nuclear potential by choosing

$$\omega_0^N = \omega_0 \left(1 + \gamma \frac{N-Z}{A}\right)$$

$$\omega_0^Z = \omega_0 \left(1 - \gamma \frac{N-Z}{A}\right)$$

where $\gamma$ is as yet undetermined.

The simplest way to determine $\gamma$ is to use the empirically fulfilled requirement that (see problem 6.12)

$$\langle r^2 \rangle_N \simeq \langle r^2 \rangle_Z$$

This leads to $\gamma \simeq 1/3$, and the resulting difference in neutron–proton potential accounts well for the Coulomb potential and the difference in the purely nuclear potential for protons and neutrons when $N \neq Z$.

Actually from the numerical calculations of the nuclear wave functions it is very easy to obtain values of $\langle r^2 \rangle_N$ and $\langle r^2 \rangle_Z$. From these numerical values, $\hbar\omega_0^N$ and $\hbar\omega_0^Z$ can be fitted so that the desired values for the radii of the neutron and proton distributions are reproduced exactly. It turns out that the original estimate of

$$\hbar\omega_0^{N,Z} = 41 \cdot A^{-1/3} \left(1 \pm \frac{1}{3} \frac{N-Z}{A}\right) \text{ MeV}$$

is correct within 1–2% for all nuclei with exception of the very lightest ones.

## 6.4 Single-particle spectra of closed-shell ± 1 nuclei – the parameters κ and μ′

Nuclei having doubly closed shells apart from one added neutron or one added proton or one missing neutron (a neutron hole) or one missing proton (a proton hole) are the nuclei for which the single-particle picture should be

particularly appropriate. This is so first because these nuclei are spherical and we have limited our calculations to the case of good spherical symmetry. Furthermore, with several particles outside a closed shell and occupying an incompletely filled subshell, the 'residual forces' (interactions not taken care of by the average field) are, in spite of their relative smallness, decisive for the order of occurring nuclear spins in the excitation spectrum. We shall therefore take the approach that we first consider only doubly magic $\pm 1$ nuclei. For such nuclei, with the odd particle in the lowest subshell above the gap, the total angular momentum $I$ equals the $j$-value of this subshell. For example, in $^{17}_{8}O_9$, with the odd neutron in the $d_{5/2}$ shell, $I = 5/2$.

'One-hole' states are also associated with angular momentum $j$. Thus

$$I(\text{one hole}) = I(\text{one particle}) = j$$

This arises from the following argument: firstly, a closed subshell, having all positions filled, has $I = 0$. Secondly, the last particle of such a closed subshell contributes an angular momentum vector $\mathbf{j}$, which has to balance exactly the vector sum of the angular momentum of all the other particles. This can only be true if these other particles vector couple to $\mathbf{I} = \mathbf{j}$ (cf. fig. 7.3).

For doubly magic $\pm n$ nuclei (where $n$ is a small integer), we first consider the case of an even number of particles of one kind. About these we shall assume that they always couple to total angular momentum zero in the lowest energy state. This is supported by much data.

For an odd number of like particles we shall assume the 'seniority rule' (Racah, 1950) that *two by two particles of the same kind pair off to angular momentum zero.* This rule can be qualitatively understood if one introduces a residual force proportional to $\delta(\mathbf{r}_1 - \mathbf{r}_2)$ operating between the like particles in the partly filled subshell (Mayer, 1950). Then the state favoured energetically (and by definition of 'lowest seniority') is the one with particles pairing off to angular momentum zero. By this rule e.g.

$$I\left[\left(d_{5/2}\right)^3\right] = I\left(d_{5/2}\right) = 5/2$$

The spins resulting for light odd-$Z$ nuclei if the seniority rule were strictly followed are listed in table 6.1. A similar table can also be made for odd-$N$ nuclei. Note that an 'odd-$Z$' nucleus has $Z$ = odd, $N$ = even, while an 'odd-$N$' nucleus has $N$ = odd and $Z$ = even.

When comparing predicted and measured spins in table 6.1, one first notes the remarkable agreement. Indeed, the seniority rule is found to hold also for heavier nuclei if $|n|$ is kept reasonably small, say $|n| \lesssim 5$ or 7. For larger

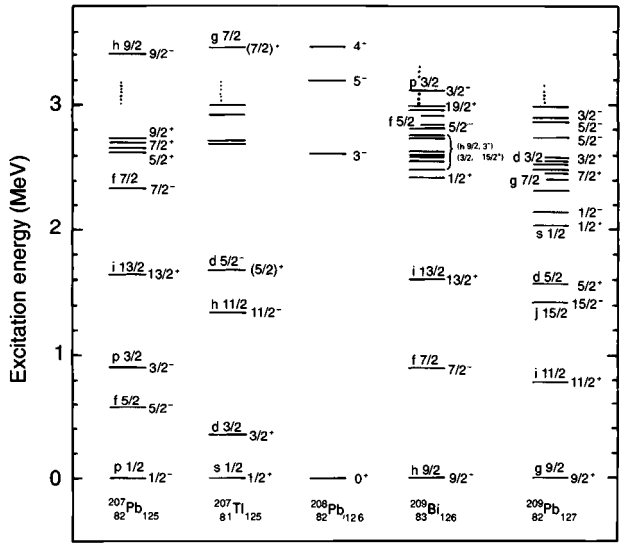


Fig. 6.5. Observed low-energy spectra for $^{208}$Pb and neighbouring one-hole and one-particle nuclei. The states are labelled by their spin and parity and, when appropriate, by the corresponding subshell of the particle or hole. The states of $^{209}$Bi formed from the $h_{9/2}$ ground state coupled to the collective $3^-$ state in $^{208}$Pb are also indicated (data from *Table of Isotopes*, ed. by C.M. Lederer and V.S. Shirley, John Wiley, 1978)

values of $|n|$, other coupling schemes might take over. For example, the nuclei with $A \simeq 20$–25, where disagreement is found in table 6.1, are described as being deformed (such nuclei are discussed first in chapter 8).

One may go further and also discuss excitation spectra for closed-shell ±1 nuclei. As an example, the observed low-energy spectra for $^{208}$Pb and the neighbouring nuclei are given in fig. 6.5. The states with the odd particle or the hole in the $j$-shells around $Z = 82$ and $N = 126$ are easy to identify. It is first for excitation energies larger than about 2 MeV that other kinds of states are observed, for example where the collective $3^-$ state of $^{208}$Pb couples to the ground state of the odd nucleus. From the spectra of fig. 6.5, the energies of the different subshells can be obtained as shown in fig. 6.6 (the energy gaps for $Z = 82$ and $N = 126$ are most easily extracted from the measured mass of $^{208}$Pb relative to $^{209}$Bi and $^{209}$Pb, respectively). In fig. 6.6 is also shown how well these energies are reproduced in a typical fit based on the Woods–Saxon potential.

We now continue to consider the energy spectra in the region of some other closed nuclei. Then, the position of the neutron subshells around $^{16}_{8}O_8$, $^{40}_{20}Ca_{20}$, $^{48}_{20}Ca_{28}$ and $^{56}_{28}Ni_{28}$ are obtained as shown in fig. 6.7. There, we also

6.1. *Shell model subshell occupation for light odd-Z nuclei. Note that the spin resulting from the sphe*
*l (Theor, I) is in agreement with observed spin (Exp, I) except for the nuclei $^{19}F$ and $^{23}Na$. These lat*
*e described as deformed where the valence nucleons fill orbitals that are superpositions of the $d_{5/2}$, $d_{3/2}$*
*orbitals.*

| ent | $Z$ | $1s_{1/2}$ | $1p_{3/2}$ | $1p_{1/2}$ | $1d_{5/2}$ | $2s_{1/2}$ | $1d_{3/2}$ | $1f_{7/2}$ | Config. | Eq. config. | Theor. $I$ | Exp $I$ |
|---|---|---|---|---|---|---|---|---|---|---|---|---|
| | 1 | 1 | | | | | | | $s_{1/2}$ | | 1/2 | 1/2 |
| i | 3 | 2 | 1 | | | | | | $p_{3/2}$ | | 3/2 | 3/2 |
| 3 | 5 | 2 | 3 | | | | | | $(p_{3/2})^3$ | $(p_{3/2})^{-1}$ | 3/2 | 3/2 |
| N | 7 | 2 | 4 | 1 | | | | | $p_{1/2}$ | | 1/2 | 1/2 |
| | 9 | 2 | 4 | 2 | 1 | | | | $d_{5/2}$ | | 5/2 | 5/2 |
| | 9 | 2 | 4 | 2 | 1 | | | | $d_{5/2}$ | | 5/2 | 1/2 |
| a | 11 | 2 | 4 | 2 | 3 | | | | $(d_{5/2})^3$ | $d_{5/2}$ | 5/2 | 3/2 |
| l | 13 | 2 | 4 | 2 | 5 | | | | $(d_{5/2})^5$ | $(d_{5/2})^{-1}$ | 5/2 | 5/2 |
| | 15 | 2 | 4 | 2 | 6 | 1 | | | $s_{1/2}$ | | 1/2 | 1/2 |
| l | 17 | 2 | 4 | 2 | 6 | 2 | 1 | | $d_{3/2}$ | | 3/2 | 3/2 |
| l | 17 | 2 | 4 | 2 | 6 | 2 | 1 | | $d_{3/2}$ | | 3/2 | 3/2 |
| K | 19 | 2 | 4 | 2 | 6 | 2 | 3 | | $(d_{3/2})^3$ | $(d_{3/2})^{-1}$ | 3/2 | 3/2 |
| K | 19 | 2 | 4 | 2 | 6 | 2 | 3 | | $(d_{3/2})^3$ | $(d_{3/2})^{-1}$ | 3/2 | 3/2 |
| c | 21 | 2 | 4 | 2 | 6 | 2 | 4 | 1 | $f_{7/2}$ | | 7/2 | 7/2 |
| | 23 | 2 | 4 | 2 | 6 | 2 | 4 | 3 | $(f_{7/2})^3$ | $f_{7/2}$ | 7/2 | 7/2 |
| n | 25 | 2 | 4 | 2 | 6 | 2 | 4 | 5 | $(f_{7/2})^5$ | $f_{7/2}$ | 7/2 | 7/2 |
| o | 27 | 2 | 4 | 2 | 6 | 2 | 4 | 7 | $(f_{7/2})^7$ | $(f_{7/2})^{-1}$ | 7/2 | 7/2 |

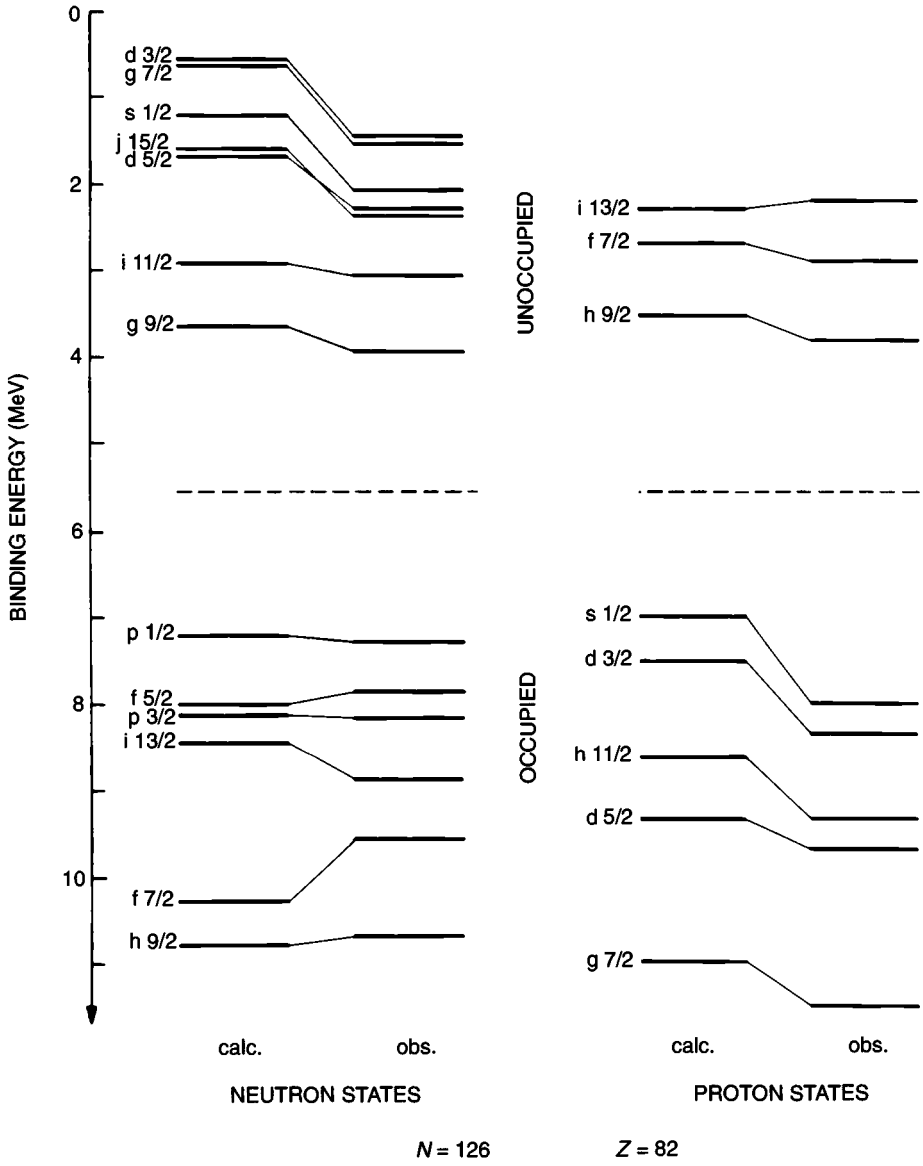


Fig. 6.6. The single-neutron and single-proton levels obtained from the spectra of nuclei near the double-magic nucleus $^{208}$Pb (fig. 6.5). The experimental levels are exhibited to the right in each case. They are compared with the single-particle levels obtained from the fit by Blomqvist and Wahlborn (*Arkiv Fysik* **16** (1960) 545) based on a Woods–Saxon potential (from Bohr and Mottelson, 1969).

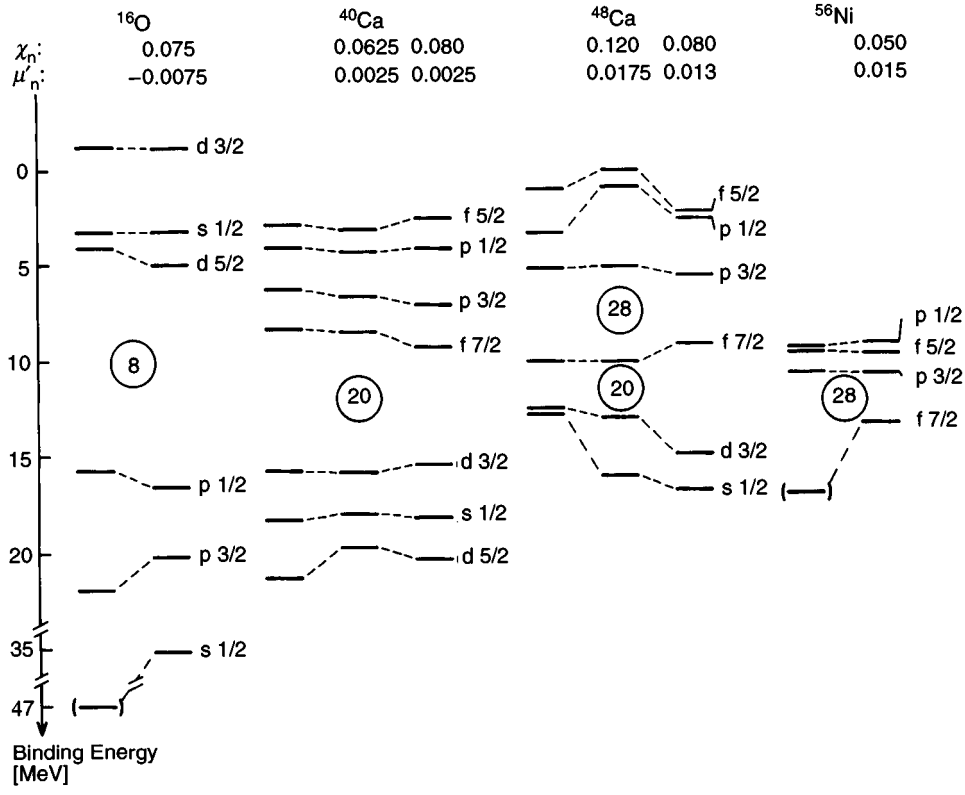


Fig. 6.7. Single-neutron energies around ${}^{16}_{8}O_8$, ${}^{40}_{20}Ca_{20}$, ${}^{48}_{20}Ca_{28}$ and ${}^{56}_{28}Ni_{28}$. The experimental values shown to the right in each figure are taken from the adjacent odd-$N$ isotopes such as ${}^{15}O$, ${}^{17}O$ etc. The modified oscillator fits are identified by the values of $\kappa$ and $\mu'$ $(= \kappa\mu)$ listed above the spectra. Where two fits are exhibited, as for ${}^{40}Ca$ and ${}^{48}Ca$, they correspond to different weightings of the observed levels.

give the energy levels obtained from fits of the modified oscillator (MO) parameters, $\kappa$ and $\mu$ (or $\mu'$). Such fits are straightforward because, from the formulae given in this chapter, it is easy to write down the energy levels of the spherical MO potential in closed form,

$$E(N\ell j) = \hbar\omega_0 \left[ N + \frac{3}{2} - \kappa \begin{Bmatrix} \ell \\ -(\ell+1) \end{Bmatrix} - \mu' \left( \ell(\ell+1) - \frac{N(N+3)}{2} \right) \right] \quad \begin{cases} j = \ell + \frac{1}{2} \\ j = \ell - \frac{1}{2} \end{cases}$$

In fig. 6.7, one could note that, to fit in a satisfactory way the spectra of both ${}^{40}Ca$ and ${}^{48}Ca$, the parameter $\mu'$ must be chosen substantially larger in the latter nucleus.

Table 6.2. *Values of the modified oscillator parameters $\kappa$ and $\mu$ as suggested by Bengtsson and Ragnarsson (1985). $\kappa$ is the strength of the $\ell\cdot$ s-term and $\kappa\cdot\mu$ $(=\mu')$ is the strength of the $\ell^2$-term.*

| $N$ | Protons | | Neutrons | |
|---|---|---|---|---|
| | $\kappa$ | $\mu$ | $\kappa$ | $\mu$ |
| 0 | 0.120 | 0.00 | 0.120 | 0.00 |
| 1 | 0.120 | 0.00 | 0.120 | 0.00 |
| 2 | 0.105 | 0.00 | 0.105 | 0.00 |
| 3 | 0.090 | 0.30 | 0.090 | 0.25 |
| 4 | 0.065 | 0.57 | 0.070 | 0.39 |
| 5 | 0.060 | 0.65 | 0.062 | 0.43 |
| 6 | 0.054 | 0.69 | 0.062 | 0.34 |
| 7 | 0.054 | 0.69 | 0.062 | 0.26 |
| 8... | 0.054 | 0.60 | 0.062 | 0.26 |

By fitting the level spectra of well-established spherical nuclei near the double-magic cases, $(Z = 8, N = 8)$, $(Z = 20, N = 20)$, $(Z = 20, N = 28)$, $(Z = 28, N = 28)$, $(Z = 50, N = 82)$, and finally $(Z = 82, N = 126)$, one obtains sets of $\kappa$ and $\mu'$ for neutrons and protons valid in different parts of the nuclear periodic table. As illustrated in fig. 6.7, however, the agreement between calculated and experimental energies is far from perfect and similar fits can be obtained for rather different values of $\kappa$ and $\mu'$. Furthermore, the 'observed energies' extracted from closed-shell ±1 nuclei appear to include some correlations and are thus not the bare energies we want to calculate in a single-particle potential. Therefore, and also because of the approximate nature of the MO potential, we can only get a rough determination of $\kappa$ and $\mu'$.

A better way to obtain $\kappa$ and $\mu'$ is through a fit to known single-particle levels in the well-established deformed regions $20 \leq A \leq 28, 150 \leq A \leq 190$ and $A > 225$ (see e.g. figs. 11.5 and 11.6 below). A criterion for the usefulness of the potential is the fact that the variations of $\kappa$ and $\mu'$ with $N$ and $Z$ are small and fairly continuous (see e.g. Nilsson *et al.*, 1969).

When doing calculations with the MO potential one could use two somewhat different strategies. The same values of $\kappa$ and $\mu'$ (or $\mu$) could be used for all shells, leading to a potential only applicable to a limited region of nuclei. The other possibility is to use different values of $\kappa$ and $\mu'$ for different $N$-shells as exemplified in fig. 6.3. Values from a more recent fit are listed in

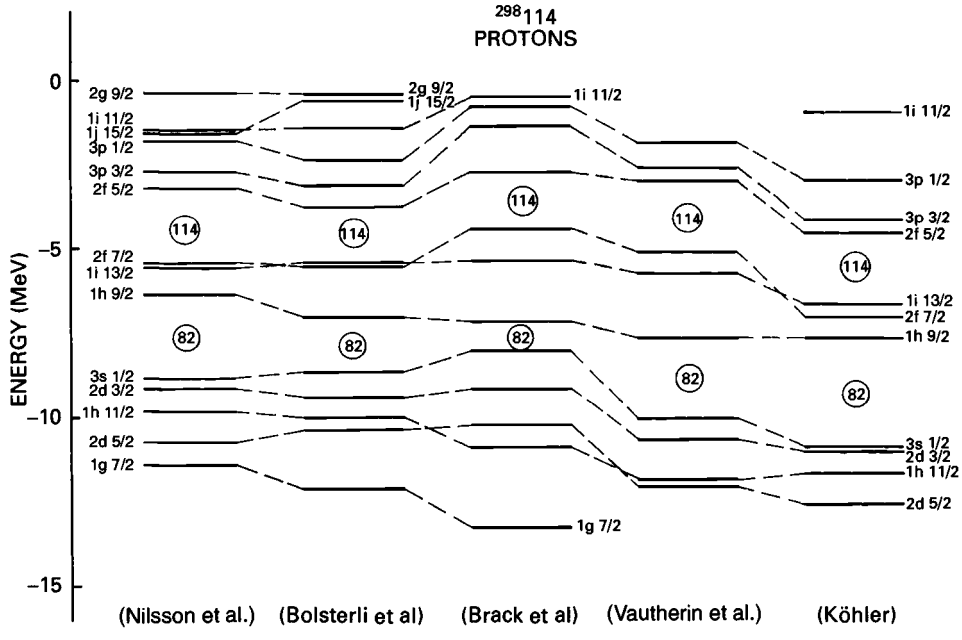


Fig. 6.8. Single-proton levels predicted in the $^{298}114$ region. The predictions are based on the modified oscillator potential (S.G. Nilsson *et al., Nucl. Phys.* **A131** (1969) 1), Woods–Saxon type potentials (M. Bolsterli, E.O. Fiset and J.R. Nix, *Physics and Chemistry of Fission*, IAEA, Vienna, 1969, p. 183; M. Brack, J. Damgaard, A. Stenholm-Jensen, H.C. Pauli, V.M. Strutinsky and C.Y. Wong, *Rev. Mod. Phys.*, **44** (1972) 320) and Hartree–Fock calculations (D. Vautherin, M. Vénéroni and D.M. Brink, *Phys. Lett.* **33B** (1970) 381; M.S. Köhler, *Nucl. Phys.* **A170** (1971) 88).

table 6.2. With $\kappa = \kappa(N)$ and $\mu = \mu(N)$, it is possible to construct a potential that approximately reproduces the level order around the Fermi surface for all nuclei. As only the orbitals around the Fermi surface influence most measurable properties, the two strategies are essentially equivalent when a limited region of nuclei is studied. The latter strategy, however, has the advantage that the same potential can be used for all nuclei.

## 6.5 The prediction of nuclear shells at $Z = 114, N = 184$

An interesting problem that presents itself is the possibility of predicting other closed shells beyond neutron and proton numbers corresponding to existing nuclei. The hope is then that the associated shell effects (see chapter 9) are large enough to lead to nuclei with a relative longevity (e.g. $t_{1/2} > 1$ year) with respect to fission and alpha decay.

As seen in fig. 6.8 the next proton shell beyond $Z = 82$ appears to occur

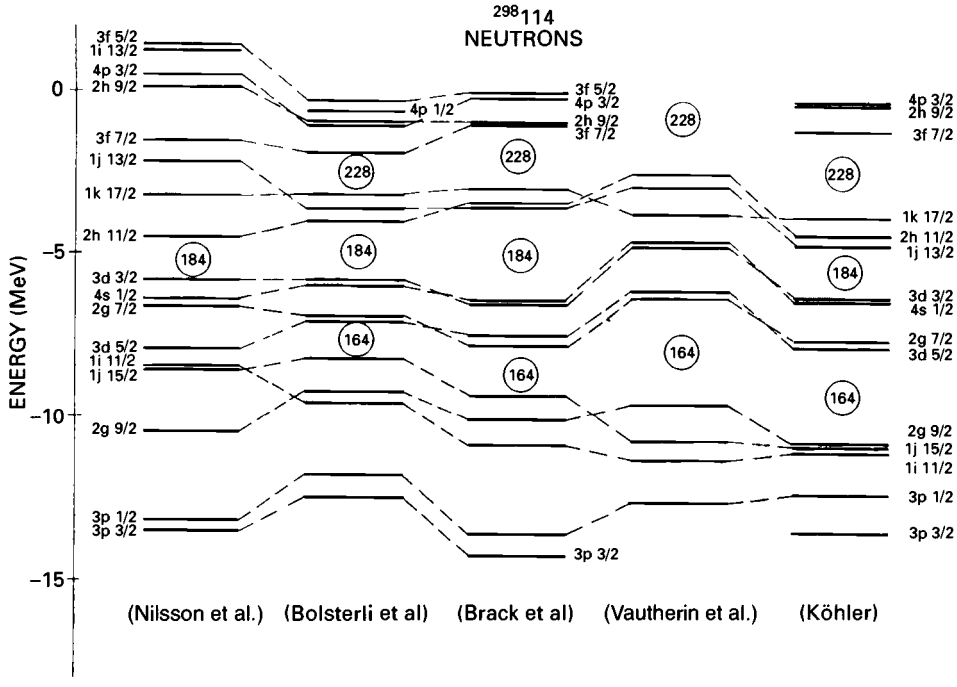


Fig. 6.9. Same as fig. 6.8 but valid for the neutron levels.

for $Z = 114$ and corresponds to a splitting of the 5f shell between $f_{5/2}$ and $f_{7/2}$. This prediction is common to the MO potential, Woods–Saxon type potentials and also the potentials derived from Hartree–Fock calculations. The magnitude of the shell effect is, however, highly dependent on how the spin–orbit strength extrapolates with $A$. Thus, even if all calculations in fig. 6.8 predict a large 114 gap, they are rather different in other ways, which hints that the uncertainties in the extrapolations are large.

The next neutron shell corresponds to $N = 184$ in most extrapolated nuclear potentials (see fig. 6.9). Here the position of a subshell $h_{11/2}$ above $N = 184$ is critical to the size of the $N = 184$ gap. In the MO potential, the $h_{11/2}$ subshell occurs right in the middle of a gap between $d_{3/2}$ and $k_{17/2}$. The shell $N = 196$, above $h_{11/2}$, is then as important as $N = 184$. In the alternative Woods–Saxon type potentials, as seen in fig. 6.9, the 184 gap dominates clearly over the 196 gap, actually to the point of wiping the latter out.

The fits shown in figs. 6.8 and 6.9 were all obtained around 1970. In the spectrum of Köhler in fig. 6.8, one observes that the $Z = 126$ gap is about as large as the $Z = 114$ gap. Some calculations even give a larger 126 gap than 114 gap. However, the predictions of $Z = 114$ and $N = 184$ as the most

probable candidates for closed shells beyond those observed are certainly still valid.

The combination of proton number $Z = 114$ with neutron number $N = 184$ corresponds to the nucleus $^{298}114$. This nucleus or the neighbouring nuclei should then be associated with the longest half-lives. Estimates of the corresponding fission half-lives are discussed in chapter 10.

## Exercises

6.1 Carry through the substitution for the three-dimensional harmonic oscillator

$$\rho = \left(\frac{M\omega_0}{\hbar}\right)^{1/2} r$$

and

$$\frac{u(\rho)}{\rho} = R(\rho)$$

Make also the 'ansatz' (why?)

$$u(\rho) = f(\rho)\rho^{\ell+1}\mathrm{e}^{-\rho^2/2}$$

to derive the equation

$$\rho f'' + \left(2\ell + 2 - 2\rho^2\right) f' + \rho\left(\frac{2E}{\hbar\omega_0} - 2\ell - 3\right) f = 0$$

Make finally the substitution $z = \rho^2$ to show that $f(z)$ satisfies the differential equation of a confluent hypergeometrical function.

6.2 Write out the wave functions for the isotropic three-dimensional harmonic oscillator

$$\begin{aligned} N &= 0 \quad \ell = 0 \\ N &= 1 \quad \ell = 1 \\ N &= 2 \quad \ell = 0, 2 \\ N &= 3 \quad \ell = 1, 3 \end{aligned}$$

Carry through the normalisations.

6.3 Consider an infinite radial box characterised by $V(r) = -V_0$ for $r \leq R$ and $V(r) = \infty$ for $r > R$ and show that the radial eigenfunctions are given by the spherical Bessel functions $j_\ell(\xi)$ where $\xi = kr$ and $k = [2M(E + V_0)/\hbar^2]^{1/2}$.